

http://pubs.acs.org/journal/aesccq Article

# Particle- and Light-Mediated Processes Control Seasonal Manganese Oxide Cycling in a Meromictic Pond

Hayley J. Gadol, Chadlin M. Ostrander, Luciana Villarroel, Lina Taenzer, Scott D. Wankel, Véronique E. Carignan, and Colleen M. Hansel\*



Cite This: https://doi.org/10.1021/acsearthspacechem.2c00368



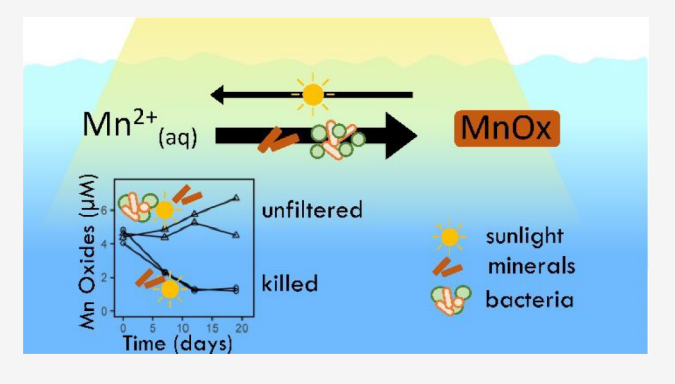
**ACCESS** I

III Metrics & More

Article Recommendations

s Supporting Information

ABSTRACT: Manganese (Mn) oxides are strong oxidants and sorbents of nutrients and contaminants, thus their formation mechanisms impact multiple biogeochemical cycles. Manganese in oxic surface waters is often found as dissolved Mn species, such as Mn(II) and Mn(III)-ligand complexes, rather than Mn oxides. This is believed to be a result of Mn oxide reduction by hydrogen peroxide associated with photolysis of organic matter and direct organic matter-mediated reduction within sunlit waters. Nevertheless, Mn oxides can persist in some surface environments, which indicates an incomplete understanding of controls on Mn oxide distributions. Here, we couple field- and lab-based analyses to explore Mn oxide distributions, Mn oxidation rates, and underlying controls on Mn oxide formation within Siders Pond, a brackish and



meromictic pond on Cape Cod (Massachusetts, USA) during the summer and fall of 2020. Manganese oxides were observed consistently in sunlit surface waters with concentrations declining to undetectable at the base of the chemocline. Surface Mn oxide concentrations were highest in late summer, reaching concentrations of  $\sim 1~\mu M$ , and lowest in late fall, reaching only  $\sim 50~n M$ . Minerals identified using synchrotron-based absorbance measurements were structurally similar to  $\delta$ -MnO<sub>2</sub> and feithnechtite. Substantial light-mediated Mn oxidation only took place in live incubations of Siders Pond water while net Mn reduction proceeded in killed incubations. Thus, total particle-mediated oxidation by microbes and minerals combined outpaced photoreduction, leading to net accumulation of Mn oxides within Siders Pond. Our results identify important roles for microbial- and mineral-mediated oxidation in determining Mn oxide distributions within surface waters of a natural setting, a finding that may help explain comparable distributions in other locations.

KEYWORDS: Manganese speciation, Manganese oxidation, Photoreduction, Birnessite, X-ray absorption spectroscopy

#### ■ INTRODUCTION

Manganese (Mn) oxide minerals are components of various particle and mineral deposits found in a wide range of environments, including desert rock varnish, mineral coatings within soils, and ferromanganese crusts and nodules in the ocean. And Manganese oxides are sorbents of nutrients and contaminants, including organic carbon, hosphate, and many trace metals. Thus, the redox cycling of Mn exerts an important control on nutrient availability, with Mn itself also acting as an important micronutrient. Manganese oxides are also strong oxidants with the ability to oxidize organic carbon either through direct interactions or indirectly via microbial respiration. Therefore, understanding mechanisms underlying Mn oxide formation and dissolution has implications for a diversity of environments and biogeochemical cycles.

Manganese exists in the environment in three redox states: Mn(II), which typically exists as an aqueous or complexed ion; Mn(III), which is either complexed with organic ligands 13,14 or hosted in Mn oxide minerals; and Mn(IV),

which precipitates as various Mn oxide phases. While the two-electron-transfer reaction of Mn(II) oxidation to Mn(IV) is thermodynamically favorable under oxic conditions, the first oxidation step from dissolved Mn(II) to Mn(III) is thermodynamically constrained at circumneutral pH. This constraint may be overcome by complexing Mn(II) with ligands; catalyzing Mn oxidation by microbes, nicluding fungi, or on mineral surfaces; or through direct Mn(II) oxidation by reactive oxygen species (ROS) like superoxide  $(O_2^{\bullet-})$ . Superoxide is produced via several photochemical and (a) biotic pathways, including via photolysis of organic

Special Issue: Environmental Redox Processes and

Contaminant and Nutrient Dynamics

Received: December 1, 2022 Revised: April 28, 2023 Accepted: May 5, 2023



 $\mathsf{matter}^{21,22}$  and extracellular reduction of oxygen by  $\mathsf{microbes.}^{23,24}$ 

Manganese oxide reduction can occur by a number of mechanisms, including by microbial respiration, <sup>25</sup> direct reduction by organic carbon, <sup>26,27</sup> and by reactions with iron(II), <sup>28</sup> sulfide, <sup>29</sup> and the ROS hydrogen peroxide ( $H_2O_2$ ). <sup>18,30</sup> Hydrogen peroxide, like superoxide, can be produced through organic matter photolysis <sup>31</sup> and by microbial activity <sup>24</sup> in aquatic systems. Direct photoreduction of hexagonal birnessite has also been observed, <sup>32</sup> but the importance of this reduction mechanism in the environment is still undetermined.

In marine systems, Mn in surface waters is predominantly found as dissolved manganese species, including Mn(II) and Mn(III) complexed with ligands. Production and persistence of these reduced dissolved Mn species in surface sunlit waters is thought to derive in large part from photoreduction of Mn oxides,<sup>36</sup> specifically through reactions with photoproduced H<sub>2</sub>O<sub>2</sub>. Additionally, diel cycling of Mn has been observed, with faster rates of Mn(II) oxidation observed at night than during the day in coastal waters near the Bahama Islands.<sup>37</sup> Diel manganese cycling has also been associated with a change in particulate Mn average oxidation state (AOS) in the surface waters of the Arctic Ocean, ranging from 2.4 during the day to ~3.0 at night.<sup>38</sup> Therefore, sunlight likely plays an important role in decreasing Mn oxide concentrations and governing their distributions within surface waters. Nevertheless, studies have shown particulate Mn or Mn oxides to be the predominant Mn species in some surface waters, particularly in lakes and estuarine waters. 34,39

While photochemical and biological processes appear to play important roles in Mn cycling, their relative contributions are not well understood. Accordingly, the goal of this research was to examine temporal and spatial variability in Mn oxide profiles as influenced by biological and photochemical processes in a meromictic brackish pond (Siders Pond, Cape Cod, MA). We hypothesized that Mn oxides accumulate in Siders Pond during peak microbial productivity, allowing for microbial oxidation to occur faster than photoreduction. We tested this hypothesis through fieldwork across one seasonal transition from midsummer to late fall in 2020 and pond water incubations conducted under different conditions. Here, we highlight that the relative balance between light-mediated reduction and particle-mediated oxidation controls Mn oxide profiles and cycling in Siders Pond, which has potentially broad implications for Mn cycling in other aquatic systems.

# ■ METHODS

Field Site and Protocols. Siders Pond is a meromictic (semi-permanently stratified, does not undergo seasonal mixing) pond located in Falmouth, Massachusetts. The pond is meromictic due to inputs of denser salt water, leading to a generally permanent density gradient with depth. This is in contrast with most ponds, which are holomictic and generally undergo seasonal turnovers in spring and fall. This field site was chosen because it is a stratified yet dynamic pond with inputs from seawater and groundwater. Because Siders Pond is stratified over decadal timescales, the effect of decreasing sunlight and temperature from summer to fall on Mn cycling could be studied without the influence of seasonal turnover. There were also previously observed Mn oxides in the surface waters of the pond.

Profile samples were obtained from the southwest side of Siders Pond (~12 m) near the deepest point in the pond (Figure S1). The maximum depth of the pond is about 15 m. Profile samples were collected on July 31, August 14, August 20, September 4, September 19, November 7, and November 21, 2020. Samples were collected using a peristaltic pump operating at  $\sim$ 100 mL/min. The tubing was flushed with water from each target depth for at least 1-2 min before collecting water for analysis. About 250 mL of unfiltered water was collected for sulfide and chlorophyll analyses. For all remaining aqueous analyses, about 2 L of water was filtered via an inline Sterivex (0.22  $\mu$ m PES) filter. Samples for dissolved iron (Fe) analysis were immediately acidified to a final approximate concentration of 2% hydrochloric acid. Samples were also collected on Sterivex filters for particle-based analyses. Known volumes were filtered for Mn oxide quantification and larger volumes (200 to 1000 mL) for X-ray absorption spectroscopy (XAS). A YSI multiprobe system (556 MPS) was used to record pH, dissolved oxygen, conductivity, and salinity profiles at each date, and photosynthetically active radiation (PAR) profiles were recorded with an LI-COR Light Sensor Logger (LI-1500). Normalized PAR was calculated by dividing individual PAR observations by their respective maximum PAR value on each date to remove time-of-day effects. No unexpected or unusually high safety hazards were encountered during fieldwork or laboratory experiments.

Incubation Setup. Incubation experiments were prepared using site water collected on July 29th, August 20th, September 17th, and November 7th. All four dates included water from 1 m depth, while incubations from September 17th also included 2.5 m water and November 7th included 2 m water, which were both within the chemocline on their respective dates. A summary of the setup is provided in Table S1. Site water was kept refrigerated or in a cooler with ice packs until use within 48 h of water collection. All incubations were conducted using 80 mL aliquots of site water in 100 mL glass beakers. After all necessary additions were made, the beakers were covered with Glad brand plastic wrap to minimize evaporation and contamination but still allow transmission of at least 80% of light above 250 nm based on UV—vis measurements (Figure S2).

Incubations were conducted using unfiltered water, filtered water, and unfiltered water with added mercuric chloride. Manganese(II) chloride (MnCl<sub>2</sub>) was added to each incubation for a final added concentration of 25 to 30  $\mu$ M. Waters were incubated either in natural sunlight or covered with aluminum foil to exclude all light. All incubations were prepared in duplicate except for the July incubations. July incubations were initially carried out as preliminary incubations with single replicates but were included because these incubations still provided useful context for overall trends. Killed incubations included 80 µL of saturated mercuric chloride for a final solution of consisting of about 0.01% saturated mercuric chloride (v/v) for a final mercury concentration of about 600 mg/L mercuric chloride. Filtered incubations were prepared similarly to unfiltered incubations, except using site water filtered through a Sterivex (0.22  $\mu$ m PES) filter immediately prior to starting the incubation.

A summary of the water incubation setup is shown in Figure S3. Filtered incubations had all particles >0.22  $\mu$ m removed to allow only aqueous and/or colloidal reactions to occur. Killed (mercury amended) incubations still had particles, but the microbial community was killed and/or severely inhibited, so

aqueous and mineral-mediated processes only occur in these incubations. Unfiltered incubations allowed aqueous, mineral-mediated, and biologically mediated Mn redox reactions to occur. Dark incubations included only light-independent processes. Light incubations allowed for light-dependent processes, including photochemical reactions in filtered, killed, and unfiltered incubations and possibly Mn cycling associated with phototrophic organisms in the unfiltered incubations.

Subsamples were taken every 3 to 6 days for 20 to 25 days after the start of the incubation experiments. Prior to each sample collection, any visible manganese oxides were scraped from the bottom of the beaker using a syringe, pipet tip, and/or disposable plastic spatula, and the incubations were mixed each time a sample was taken. Then, 8 to 10 mL aliquots of the homogenized water were collected with a syringe. Finally, 3 to 5 mL water was collected for Mn oxide quantification.

Determination of Aqueous Species and Mineral Concentrations. Manganese Oxide Concentrations. Manganese oxides were measured using the leucoberbelin blue (LBB) assay<sup>40</sup> with a permanganate standard curve as conducted previously.<sup>13</sup> For field samples, Mn oxides were collected and concentrated by pumping water directly through Sterivex filters. A known volume ranging from 100 to 250 mL was collected onto the filter. Filter volumes of about 100 mL were used at time points when an initial test sample visually appeared to be dark blue, likely exceeding the linear range of the LBB assay, such as on September 17, 2020. For samples with lower concentrations of Mn oxides, about 200 to 250 mL site water was filtered for the LBB assay. Then, samples were either measured immediately or frozen until analysis.

The method of LBB addition to the filters varied depending on the Mn oxide concentrations. First, a primary reagent was made with LBB at a concentration of 0.04% in 1% acetic acid. Then, a secondary reagent was made by diluting the primary reagent 1:10 with Milli-Q water. The secondary reagent was added directly to the Sterivex filter to samples from all dates with surface Mn oxide concentrations less than  $\sim 1 \mu M$ , which was approximated visually based on a test sample in the field, to fill the entire Sterivex filter chamber, which holds 2 mL of solution. Parafilm was used to seal the bottom of the Sterivex filter to ensure that LBB did not leak out during the reaction. For samples with high Mn oxide concentrations that appeared to exceed the linear range of the LBB method, the outer plastic housing of the Sterivex filter was removed using a pipe cutter, and the filter and inner plastic housing were submerged in 15 mL of LBB inside of a 50 mL centrifuge tube.

Samples were reacted with the LBB for about 30 min to 1 h for July and August sampling events, and for approximately 2 h for all subsequent field sampling, before measuring absorbance at 620 nm on a UV-vis spectrophotometer. The molar absorptivity value was determined to be  $1.4 \times 10^{5} \,\mathrm{M}^{-1} \cdot \mathrm{cm}^{-1}$ This method has also been used previously for similar measurements on filter samples from various field sites. 13,33,41 The measured absorbance was converted to a concentration within the selected LBB volume, and then corrected to actual water concentration based on the volume of water filtered and the volume of secondary LBB reagent used. LBB reacts with both Mn(III) and Mn(IV) species, but because this method does not distinguish between Mn(III) and Mn(IV), LBB-determined concentrations are reported as Mn(IV) equivalents for consistency throughout this work. The concentration was converted to Mn(IV) oxide equivalents from permanganate equivalents by multiplying the permanganate standard-based concentration by 5/2, which was done based on the expected electrons accepted for each species (5 electrons for permanganate and 2 for Mn(IV) oxides).

This method using Sterivex filters performed comparably to samples collected on PES membrane filters (Figure S4), and the measured concentration in the water was determined to be similar regardless of volume filtered and reaction time; changing conditions such as volume filtered and reaction time led to a range of measured concentrations between 0.52 and 0.78  $\mu$ M for samples collected from the same depth on the same date (Figure S5). For incubation samples, LBB measurements were done immediately after sample collection. The primary LBB reagent was added directly to unfiltered samples at a ratio of 1:10 using a 3 or 5 mL aliquot of the sample. After reacting with the LBB for 30 to 45 min, the sample was then measured on a UV—vis spectrophotometer at 620 nm and converted to Mn(IV) oxide equivalents as above.

Dissolved Iron Speciation. Samples for dissolved Fe quantification consisted of filtered water samples acidified to 2% hydrochloric acid that were immediately refrigerated until analysis, which was carried out within 2 weeks of sample collection. Dissolved Fe was measured using the Ferrozine method. 42 For Fe(II) measurements, 1 mL of acidified sample was combined with 50  $\mu$ L of 6 M ammonium acetate, and 50  $\mu$ L of 0.01 M Ferrozine reagent. This mixture was allowed to develop for 30 min before measuring absorbance at 562 nm. Total Fe measurements were made in the same way, except with addition of 25  $\mu$ L of 1.4 M hydroxylamine and allowing the samples to sit overnight before measurement. The concentration in each sample was determined based on the absorbance compared to a standard curve made with known amounts of FeCl<sub>2</sub>, and the standard curve was prepared the same way as the total Fe samples.

Sulfide Analysis. In the field, water was collected directly from the peristaltic tubing to minimize reaction with air, and either 25  $\mu$ L (high sulfide concentrations) or 250  $\mu$ L (low sulfide concentrations) of sample was added to 6 mL of 2% zinc acetate in a scintillation vial. The vials were immediately refrigerated until analysis within 2 weeks of sample collection using the Cline method. Five mL of a solution containing 43 mM  $N_1N_1$ -dimethyl-p-phenylenediamine mono hydrochloride and 22 mM FeCl $_3$ ·6H $_2$ O dissolved in hydrochloric acid was added to each of the samples. After allowing the samples to develop for at least 45 min, absorbance was measured at 670 nm. The concentration of sulfide in each sample was determined by comparing the sample absorbance to a standard curve of known sodium sulfide concentrations.

Nitrate Analysis. Samples for nitrate quantification, which were also filtered using 0.22  $\mu$ m Sterivex filters in the field, were collected and frozen until analysis. The total concentration of nitrate and nitrite was determined by converting both species to nitric oxide (NO) and measuring the NO using a chemiluminescence NO<sub>x</sub> analyzer (Teledyne).<sup>44</sup> Nitrite concentrations were determined by adding 50  $\mu$ L of a 10 g/L sulfanilamide and 50  $\mu$ L of a 1g/L N-(1-naphthyl)ethylenediamine to a 1 mL sample, and measuring absorbance at 543 nm.<sup>45</sup> Nitrate concentrations were determined by subtracting the nitrite concentration from the total NO<sub>x</sub> concentration.

Trace Metals. Samples for dissolved trace metal analysis were collected in 15 mL centrifuge tubes and acidified using twice-distilled trace-metal-clean HCl to a final molarity of  $\sim 0.1$  M. From each centrifuge tube, a small aliquot of  $\sim 200~\mu L$  was taken, spiked with In, and constituted in 2% HNO<sub>3</sub> to a final

volume of 2 mL. Concentration data were generated using a Thermo Finnigan iCAP quadrupole Inductively Coupled Plasma Mass Spectrometer (ICPMS) located at the WHOI Plasma Mass Spectrometry Facility. Concentrations were calculated via reference to ion beam intensities obtained from a five-point calibration curve constructed from serial dilutions of a gravimetrically prepared multielement standard. Drift was monitored and corrected by normalizing to spiked indium intensities.

X-ray Absorption Spectroscopy (XAS). Sterivex filters from field and incubation samples were opened using a pipe cutter, and the filter membranes were removed from the inner housing using a scalpel. Filter membranes were cut into strips, stacked on top of each other, and attached to aluminum holders using Kapton tape. X-ray absorption near edge structure (XANES) and extended X-ray absorption fine structure (EXAFS) spectra were collected at beamline 11–2 at the Stanford Synchrotron Radiation Lightsource (SSRL) using a Si(220) monochromator ( $\Phi$  = 90) and analyzed as described in detail previously.<sup>46</sup> All spectra were collected using an internal Mn(0) foil (6539 eV) to correct the sample spectral energy for any drift and/or fluctuations in the incoming X-rays. Samples were collected using a liquid N<sub>2</sub> cryostat to avoid beam-damage or alteration of samples during spectra collection. Fluorescence data were collected using a 100-element Ge solid-state detector array with soller slits and Cr filters. Transmission and fluorescence data were collected (three to five spectra per sample) from −200 to ~+500 eV around the Mn K-edge (6539 eV). Spectra were energy aligned, averaged, background subtracted, and fit using SIXPACK.<sup>47</sup> Mn K-edge XANES spectra were fit via linear combination fitting (LCF) using  $\delta$ -MnO<sub>2</sub>, feitknechtite, and Mn(II) sorbed to microbial biomass (radiolarian) as representative Mn(IV), Mn(III), and Mn(II) standards, respectively. Mn K-edge EXAFS spectra were fit initially with a standard library containing over 30 model compounds, as done previously,<sup>4</sup> with final LCF reduced to combinations of  $\delta$ -MnO<sub>2</sub>, asbolane, sodium (triclinic) birnessite, feitknechtite, and Mn(II) sorbed to biomass because this combination of standards most closely fit the data.

# RESULTS

Fieldwork. Profile Characterization. Vertical profiles of Siders Pond were characterized over a period of five months from July to November of 2020. The pond is stratified<sup>48</sup> with a defined redox structure characterized by a sharp chemocline. Overall, on all dates except July 31st, the epilimnion waters were well-mixed with uniform oxygen concentrations over depth, underlain by a chemocline with steeply decreasing oxygen concentrations and a hypolimnion below the chemocline having no detectable oxygen (Figures 1 and 2). This is exemplified by the profiles collected on July 31st as shown in Figure 1. On July 31st, maximum concentrations of dissolved oxygen (340  $\mu$ M) and nitrate (40.1  $\mu$ M) occurred above 2 m. Dissolved oxygen concentrations decreased steadily from 2 to 5 m, below which oxygen concentrations were below 20  $\mu$ M. Also on July 31st, dissolved iron concentrations were highest (6.3 µM) at 5 m depth. Sulfide (4.3 mM) and dissolved Mn (32.8  $\mu$ M) concentrations were highest at the bottom of the profile. On July 31st, the epilimnion had somewhat lower concentrations of oxygen at the surface than intermediate depths of the epilimnion. However, the reasons for this are currently unclear and this was not explored further because the

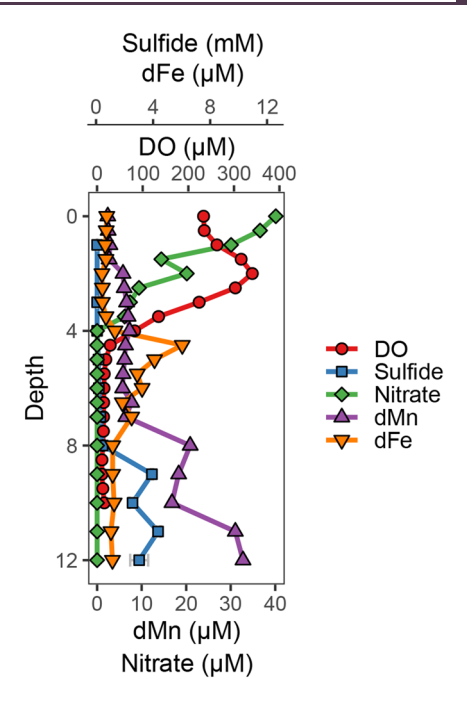


Figure 1. Profiles of select redox-active species in Siders Pond on July 31, 2020: dissolved oxygen (DO), sulfide, nitrate, dissolved Mn (dMn), and dissolved Fe (dFe).

epilimnion appeared well-mixed with respect to dissolved oxygen on subsequent sampling dates.

Even with this defined redox structure, the depth profiles of various parameters, including temperature, conductivity, pH, and dissolved oxygen changed over the course of the field season (Figure 2). The chemocline depths changed over time, with the top and bottom of the chemocline rising from 2.5 and 5.0 m in July to 1.0 and 2.5 m in November, respectively. The oxygen concentrations above the chemocline also changed seasonally. The maximum dissolved oxygen concentration was about 450  $\mu$ M in July and August, and the concentration decreased to 190  $\mu$ M by the end of November. In contrast, surface layer dissolved organic carbon (DOC) was consistent between 165 and 270  $\mu$ M with more variation within each profile than between dates (Figure S6).

A few parameters, like temperature and conductivity, were generally constant with depth within the epilimnion on any given date (Figure 2). The temperature above the chemocline decreased from 27.5 °C in July to 10.9 °C in late November. Below the chemocline, temperatures at 5 m stayed relatively constant at about 22 °C from July through September, before decreasing to 16.3 °C at 3.5 m in November. The highest temperatures in individual profiles occurred above the chemocline in July while the highest temperatures in individual profiles occurred below the chemocline in November. The conductivity, in contrast, was always lower above the chemocline than below, with the conductivity profiles staying roughly consistent over time at values of 8 to 11 PSU above the chemocline and values of 14 to 18 PSU below the chemocline.

Unlike temperature and conductivity, pH and PAR varied within the surface layer (Figure 2). In late July through mid-August specifically, pH values were slightly lower at the surface than at a depth of 2 m, where maximum pH values on those dates occurred. The highest overall observed pH value of 8.99 occurred on August 14th at a depth of 1.5 m while the lowest

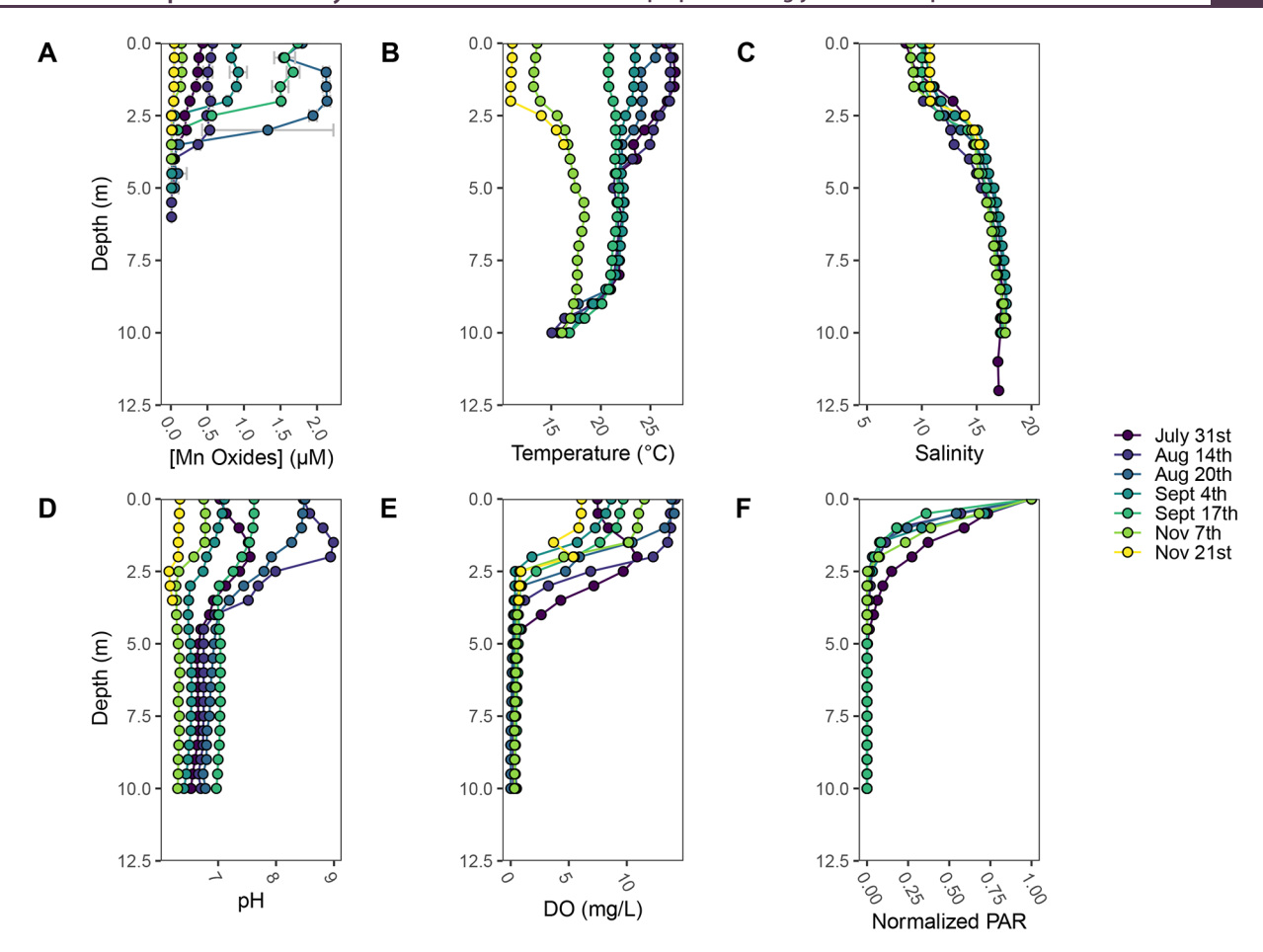


Figure 2. Profiles of particulate leucoberbelin blue (LBB)-determined manganese oxide concentration (Mn(IV) equivalents) (A), temperature (B), salinity (C), pH (D), dissolved oxygen (E), and photosynthetically active radiation (PAR) (normalized to surface values) (F) profiles in Siders Pond from July to November 2020. As the YSI and PAR sensors only had 10 m cables, many measurements were only made to a depth of 10 m.

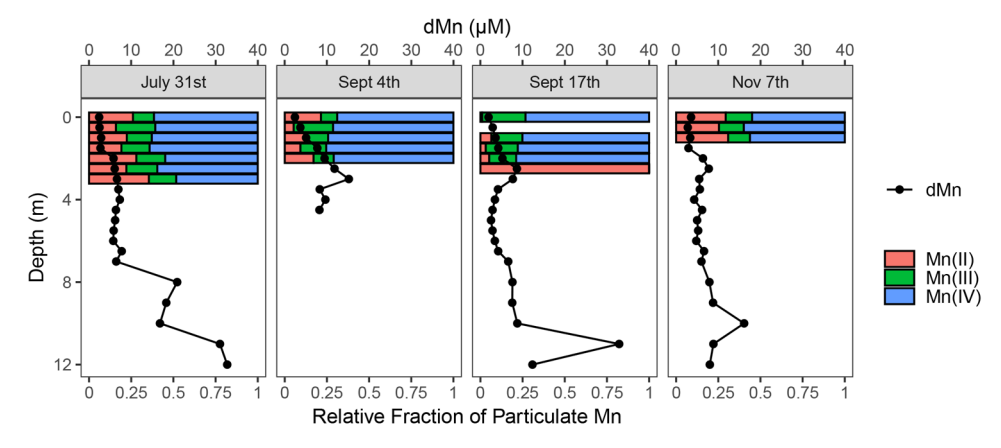


Figure 3. X-ray absorption near edge structure (XANES) spectroscopy-determined oxidation state profiles and ICP-MS-determined dissolved manganese (dMn) concentrations (black circles) from Siders Pond from July through November.

pH value of 6.15 was observed on November 21st at a depth of 3.5 m. pH values below the chemocline varied less than those above the chemocline, with a range from 6.15 to 7.04. Normalized PAR was always highest at the surface and decreased with depth. The rate of decrease with depth varied by date, and changes in normalized PAR followed no consistent trends over time.

Manganese Chemistry. Manganese oxide concentrations in Siders Pond varied with depth and by over an order of

magnitude throughout the course of the season (Figure 2A). Manganese oxide concentrations, which are reported as Mn(IV) equivalents throughout this work, were always highest and relatively uniform with depth in the surface layer and decreased throughout the chemocline, reaching undetectable concentrations below the chemocline. Surface Mn oxide concentrations in late July were  $\sim$ 0.4  $\mu$ M, and concentrations increased to a maximum of 2.1  $\mu$ M at a depth of 1 m by August 20th. Substantial concentration changes were observed on the

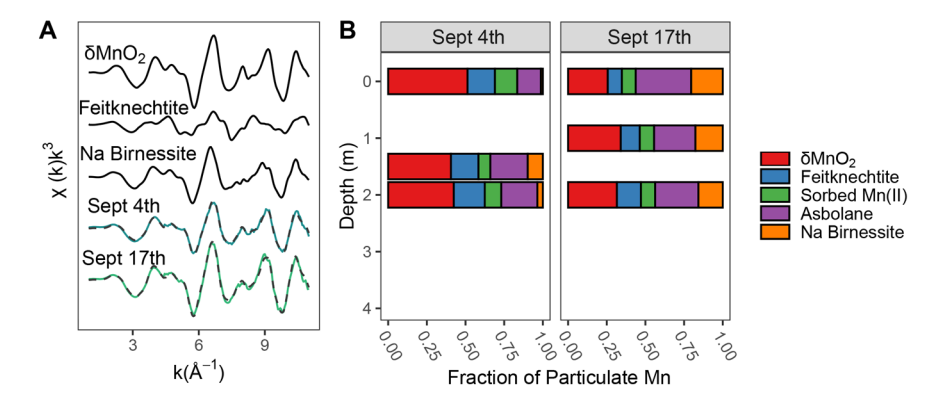
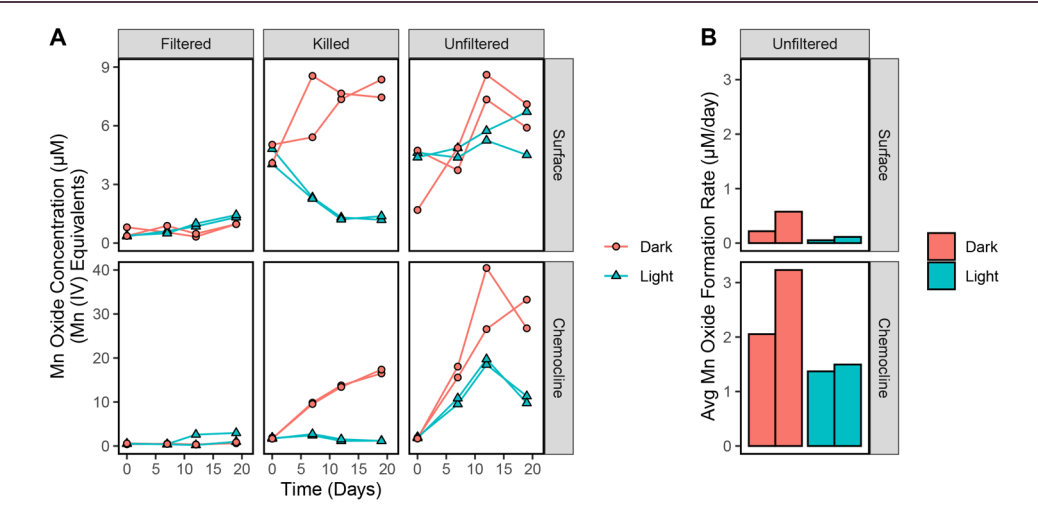


Figure 4. Extended X-ray absorption fine structure (EXAFS) spectra of selected standards and surface samples fit with combinations of standards (A) and linear combination fitting (LCF) results of profile sample EXAFS (B). In (A) sample data is depicted with solid lines while model fits are represented as dotted lines.



**Figure 5.** Changes in LBB-determined Mn oxide concentrations in September incubation experiments (A) and rates of manganese oxidation in unfiltered incubations during the first 12 days (B). Note difference in *y*-axes between surface and chemocline incubations in (A). Each line in A or bar in B represents on replicate.

time scale of weeks, with an increase in Mn oxide concentrations from about 0.6  $\mu$ M on August 14th to 2  $\mu$ M on August 20th. This was followed by a decrease to 0.9  $\mu$ M on September 4th, with another increase up to 1.7  $\mu$ M by September 17th. Surface Mn oxide concentrations were lowest in November, with concentrations as low as 50 nM on November 21st.

Relationships between Mn oxides and other measured parameters were examined via principal component analysis (PCA) using many of the measured variables normalized to their highest concentrations (Figure S7). Only variables measured across all dates and depths, which included LBBbased Mn oxide measurements, PAR, dissolved oxygen, pH, conductivity, and salinity, were included in PCA analysis. PC1 and PC2 explained 61% and 21% of the variance, respectively. Samples generally clustered by depth parallel to PC1 (Figure S7A) and date parallel to PC2 (Figure S7B). PC1 was mainly negatively associated with dissolved oxygen and PAR, and positively associated with salinity and depth. PC2 was most closely associated with temperature. The Mn oxide loadings were not parallel to either of the first two principal components or the loadings of any other measured variables. The Mn oxide loadings were most closely aligned with pH and dissolved

oxygen, and there was no loading that was anticorrelated with the Mn oxide loading.

X-ray absorption spectroscopy was used to further characterize the particulate Mn present in Siders Pond over time. Linear combination fits of the XANES data indicated that the particulate manganese across all dates and depths consisted of about 50 to 80% Mn(IV), except for one sample at the bottom of the chemocline on September 17th that was entirely Mn(II) (Figure 3). The average oxidation state of the remaining samples ranged from 3.13 to 3.75 (Figure 3, Table S2). The highest average oxidation state above the chemocline (3.75) was observed on September 17th while the lowest average oxidation state above the chemocline (3.25) was observed on November 7th. The difference between the lowest and highest average oxidation state was mostly attributed to differences in Mn(II) content, with an average Mn(II) content of 4% on September 17th (excluding the exclusively Mn(II) sample) and 25-30% on November 7th. When the Mn(II) is removed to investigate changes specifically in Mn oxides, the average oxidation state of the remaining particulate Mn was consistent across all dates between 3.7 and 3.8 (Table S2).

A subset of samples containing higher Mn oxide concentrations analyzed via EXAFS indicated that particles were composed of predominantly birnessite-like phases,

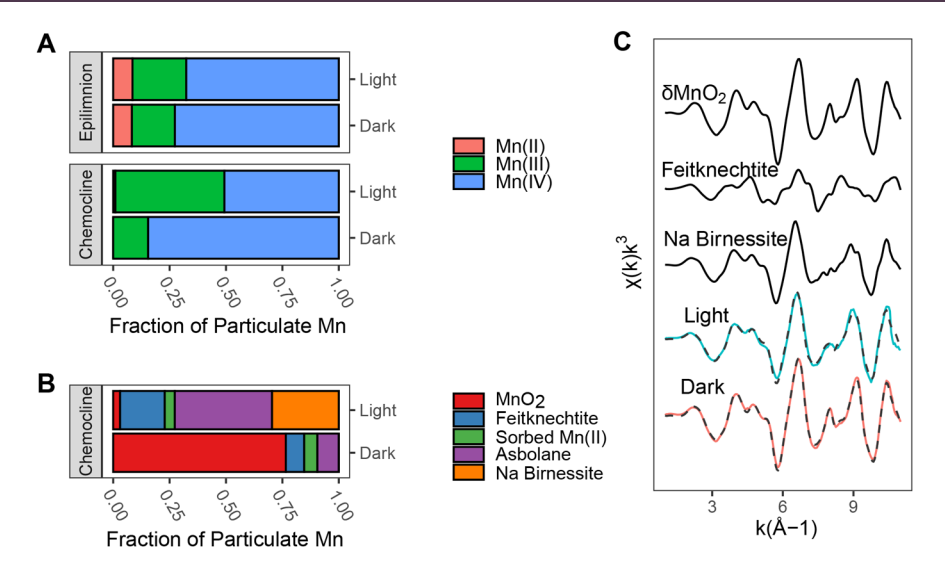


Figure 6. X-ray absorption spectroscopy (XAS) data from day 19 of September incubation experiments. XANES LCF fitting results from the epilimnion and chemocline incubations (A), EXAFS LCF fitting results (B), and EXAFS spectra with selected standards (C) from chemocline incubations.

including  $\delta$ -MnO $_2$  triclinic birnessite, and asbolane (Figure 4B). The Mn(III) oxide feitknechtite and Mn(II) were also present in the particles (Figure 4B). The  $\delta$ -MnO $_2$  content decreased from on average 45% on the 5th to 30% on the 17th, and this corresponded primarily with an increase in triclinic birnessite and asbolane. This change is apparent in the EXAFS spectra, with a dampening of the oscillation at ~7 Å (Figure 4A). This oscillation is also seen in the  $\delta$ -MnO $_2$  standard but not the triclinic birnessite or feitknechtite standards and has been referred to as an indicator region differentiating hexagonal from triclinic birnessite.

**Incubation Experiments.** Manganese Oxide Formation over Time. Incubation experiments of Siders Pond water carried out over the course of the field season elucidated underlying controls on Mn oxide formation in Siders Pond (Figures 5 and 6). To understand the role of particles, including both minerals and microbes, unfiltered incubations were compared to filtered incubations. To differentiate between mineral-mediated and microbially mediated processes associated with particles, killed incubations were compared to unfiltered incubations. Incubations were exposed to sunlight and covered in foil to exclude light for each of the three conditions (filtered, killed, and unfiltered) to determine the role of light in the presence and absence of mineral-mediated and microbially mediated Mn cycling. Light and temperature data during these incubations are shown in Figures S9 and S10 respectively.

Of incubations using waters collected in September, filtered waters produced the lowest concentration of Mn oxides (Figure 5A, left, as Mn (IV) equivalents). There was on average about 500 nM manganese oxides in the initial filtered waters from both depths. Filtered surface and chemocline water incubations formed slightly more Mn oxides in the light compared to those in the dark. Within the surface waters, the concentration of Mn oxides in the light filtered water incubations reached between 1.3 and 1.4  $\mu$ M, while dark filtered water incubations only reached 1.0  $\mu$ M on average. Within the chemocline water incubations, the Mn oxide concentrations over the course of the filtered incubations responded similarly, with light incubations reaching an average

of 2.0  $\mu$ M and dark incubations reaching an average of 0.7  $\mu$ M. In contrast, killed water incubations accumulated higher Mn oxide concentrations in the dark than in the light (Figure 5A, middle). In dark surface killed water incubations, Mn oxide concentrations increased from on average 4.4  $\mu$ M initially to about 7.5  $\mu$ M over the course of the 20-day incubation. In light surface killed water incubations, Mn oxide concentrations decreased to 1.3  $\mu$ M on average. In chemocline killed water incubations, which started with lower Mn oxide concentrations of about 1.9  $\mu$ M, there was also net oxidation in the dark and net reduction in the light. Mn oxide concentrations in dark incubations increased to 16.9  $\mu$ M, while they decreased to 1.2  $\mu$ M in the light.

Like the killed water incubations, net oxidation occurred within dark unfiltered water incubations (Figure 5A, right). However, unlike in killed water incubations, there was also net oxidation in the light, although to a lesser extent than in the dark. In surface water dark unfiltered incubations, Mn oxide concentrations increased from 3.1 µM to an average concentration of 8.0  $\mu$ M at its peak on day 12. In contrast, there was only a slight increase in Mn oxide concentrations in the light, from 4.5  $\mu M$  to 5.6  $\mu M$  on average. In chemocline unfiltered water incubations, there was also an increase from initial Mn oxide concentrations of about 2  $\mu$ M in both the light and the dark, to about 30  $\mu$ M in the dark and 10  $\mu$ M in the light. It is of note that the light unfiltered chemocline water incubations reached a pH of 8.99, and light unfiltered surface water incubations reached a pH of 8.33 over the course of the incubation, while all other incubations had a final pH of between 8 and 8.2. The measured pH values of the water in the field on September 17th at 1 and 2.5 m were 7.60 and 7.26 respectively.

Net oxidation rates in both the light and dark incubations were faster in chemocline water incubations than surface water incubations (Figure 5B). Average oxidation rates in the surface water incubations were 0.4  $\mu$ M/day and 0.1  $\mu$ M/day in the dark and light, respectively. In chemocline water incubations, Mn oxidation rates of 1.4  $\mu$ M/day in the light and 2.6  $\mu$ M/day in the dark were observed.

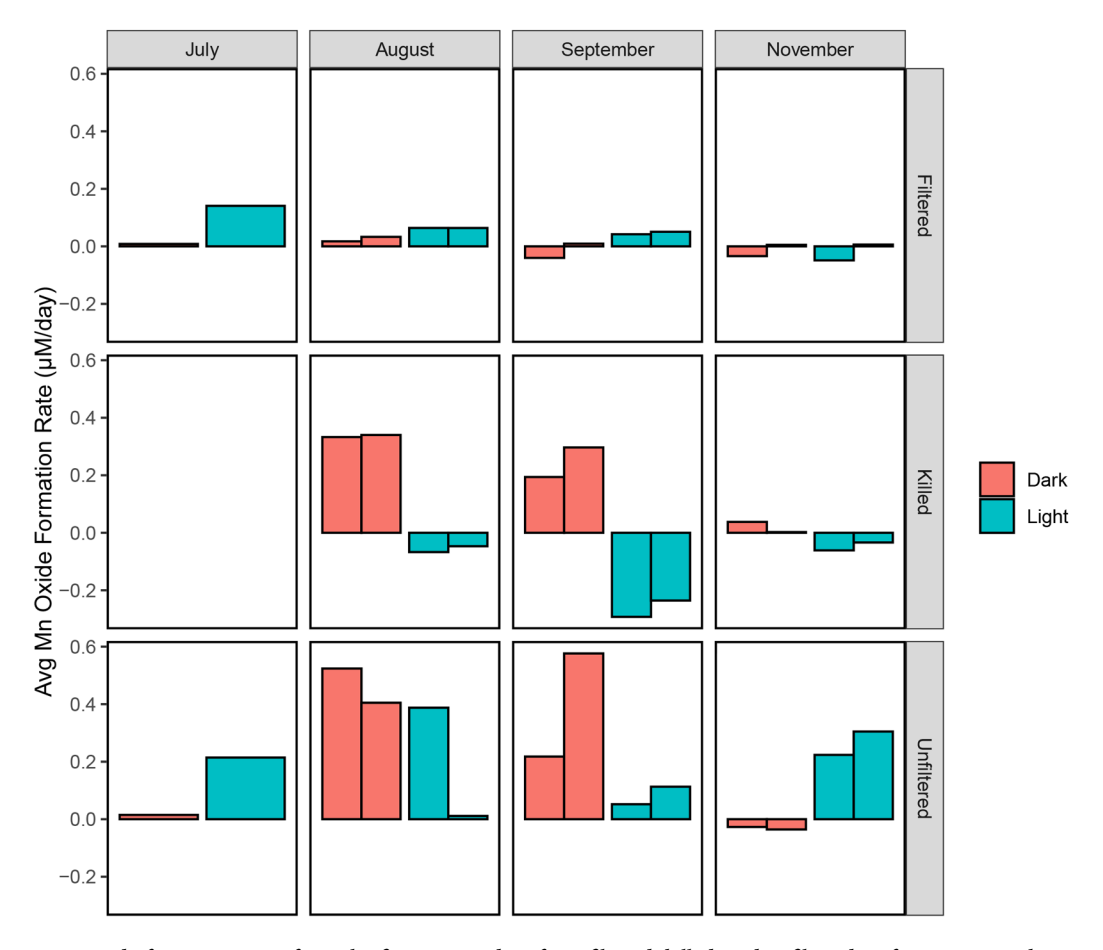


Figure 7. Manganese oxide formation rates from the first 10–13 days from filtered, killed, and unfiltered surface water incubation experiments in July through November. Killed incubation experiments were only done in August, September, and November. Each bar is one replicate. Experiments in July had one replicate while all other months had two replicates.

Particulate Manganese Characterization. Particles collected at day 19 of the unfiltered water incubations consisted predominantly of Mn(IV) and Mn(III) (Figure 6). Average oxidation states were generally lower in the light than in the dark, but with more pronounced differences arising in the chemocline water incubations (Figure 6A). Average oxidation states in surface water incubations were 3.64 in the dark, compared with 3.59 in the light, while average oxidation states in chemocline incubations were 3.84 in the dark and 3.50 in the light (Table S3). Additionally, the surface water incubations had relatively greater proportions of Mn(II), with 5–10% Mn(II), while chemocline water incubations consisted of <1% Mn(II). Light chemocline water incubations particularly contained a large proportion of Mn(III) relative to other samples, with 48% Mn(III).

Like the profile samples, chemocline water incubation particles consisted predominantly of birnessite-like phases (Figure 6 B and C). However, the specific Mn oxide composition varied between incubations. Oxides formed in the light incubations consisted predominantly of asbolane, feitknechtite, and triclinic birnessite with little  $\delta$ -MnO<sub>2</sub>, while the dark incubation oxides consisted of 75%  $\delta$ -MnO<sub>2</sub>. This is apparent in the EXAFS spectra, where a more prominent oscillation at about 7 Å is present in the dark incubations compared to those formed in the light.

Comparison of Monthly Incubation Experiments. Average dark and light net oxidation rates in both monthly incubations varied between sampling times. Net oxidation in light filtered

water incubations reached maximum rates of 0.1  $\mu$ M/day in July and decreased throughout the season to a minimum of essentially no detectable net oxidation in November (Figure 7). Oxidation rates in dark filtered water incubations were more similar over the same time frame and were close to 0  $\mu$ M/day consistently.

Killed water incubations, which were only done in August, September, and November, showed relatively consistent trends across the seasonal transition from summer to fall. There was always net oxidation in the dark and net reduction in the light. Dark killed water oxidation rates were between about 0.2 and 0.4  $\mu$ M per day. Mn oxide concentrations in light killed water incubations decreased at rates between about 0.05 and 0.3  $\mu$ M per day.

Dark unfiltered surface water oxidation rates were consistently higher than killed water and filtered water net oxidation rates in the dark. Dark unfiltered water oxidation rates were generally between 0.3 and 0.6  $\mu$ M/day, except in July and November when they were <0.1  $\mu$ M/day. Average light unfiltered water oxidation rates were consistently 0.3  $\mu$ M/day or less; in August, these rates were more variable and averaged to zero within error between the duplicates. However, substantial net reduction of the initial Mn oxides present was never observed, unlike in the killed water incubations. There was generally more variability between the two replicates in unfiltered water incubations than in filtered and killed water incubations.

#### DISCUSSION

Mn Speciation in Siders Pond. We found that Mn oxides were present consistently in Siders Pond over a period from late-July to mid-November of 2020. The Mn oxide profiles in Siders Pond were quite different from many observed marine profiles thus far, which generally exhibit substantially higher concentrations of dissolved manganese than Mn oxides in surface waters within the euphotic zone. However, like in Siders Pond, Mn oxides in surface waters at concentrations equal to or higher than dissolved manganese concentrations have been observed recently in other coastal/inland waters. Jan. 24,39

The concentrations of surface water Mn oxides in Siders Pond varied over an order of magnitude from ~50 nM in late November to 2  $\mu$ M in mid-August (Figure 2). The Mn oxide concentrations observed in July through September (see Figure 2) were comparable to those found in brackish waters in other studies, which ranged from about 0.5 to 3  $\mu$ M. The Mn oxide concentrations generally did not change with depth in epilimnion waters, indicating that mixing was a controlling factor in Mn oxide profiles. Below the epilimnion, however, Mn oxide concentrations decreased rapidly within the chemocline, ultimately reaching levels below detection at the base of the chemocline.

Methodological changes made over the course of the season may have added some uncertainty to the measured Mn oxide concentrations, but these uncertainties are much smaller than the observed variability in Siders Pond and thus highly unlikely to influence our overall conclusions. The LBB method used in this work was modified from an existing protocol applied previously to other water bodies. <sup>13,33,41</sup> Our initial LBB development time was 30 min to 1 h in July and August, but this was changed to 2 h in September. Tests of this longer development time revealed only slightly higher measured Mn oxide concentrations (Figure S5), up from 0.52  $\mu$ M to 0.78  $\mu$ M for the same Siders Pond water sample. Compare this to the two orders-of-magnitude particulate Mn oxide concentration variability observed during the course of our study (again, ~50 nM to ~2  $\mu$ M).

In contrast with the Mn oxide profiles, dissolved Mn concentrations were low at the surface and generally increased with depth below the chemocline (Figure 3) pointing to a sedimentary Mn source. Like Mn oxides, epilimnion dissolved manganese concentrations were generally uniform above the chemocline, also likely due to mixing of the surface waters.

Seasonal Transitions in Mn Oxide Cycling. While Mn oxides were consistently present and evenly distributed in the epilimnion, Mn oxide concentrations in the surface waters varied over time (Figure 2). The surface Mn oxide concentrations increased throughout the season from late July to mid-September but were about an order of magnitude lower in November than September. Despite changing environmental conditions including temperature, pH, DOC, and chemocline depth, no measured environmental variables directly correlated with the changing Mn oxide concentrations in the surface waters of Siders Pond (Figure S7 and S8). Nevertheless, while Mn oxide concentrations did not correlate with temperature above 20 °C, surface Mn oxide concentrations of 200 nM or lower were only associated with temperatures below 18 °C.

DOC concentrations in Siders Pond increased markedly at approximately 12 m depth in July (Figure S6). The depth of

ı

the pond at our sampling site was  $\sim 13$  m, thus it is possible that there was some influence from the diffusion of porewater due to the proximity of the sample to the sediment-water interface. However, this increase at 12 m was in agreement with the results from a previous study that targeted a deeper pond site ( $\sim 15$  m), <sup>51</sup> making sediment influence unlikely. DO concentrations were relatively uniform above the chemocline across all sampling dates, except on July 31st (Figure 2), and pH also increased on this day, at approximately the same depth (see Figure 2). Additional work is required to better understand these trends, but two possible explanations are (1) oxygen consumption close to the pond surface or (2) a phytoplankton bloom in the middle of the epilimnion.

The observed changes in Mn oxide concentrations in Siders Pond were accompanied by changes in average Mn oxidation rates in monthly incubation experiments (Figure 7). While all incubation experiments were only carried out in duplicate, and thus have limited statistical power, they suggest interesting trends. Mn oxidation rates in light-exposed filtered incubation experiments decreased throughout the year from July to November while Mn oxidation rates in dark filtered water incubations stayed consistent at lower values than the light oxidation rates. There was similar variation in killed water incubations, with dark oxidation rates also decreasing from September to November. There was more variation in oxidation rates in unfiltered light and unfiltered dark water incubations than in killed water incubations, with generally larger variations between duplicates and no consistent trends across the season. This may be due to the unpredictability of microbial community growth and increased temperatures in incubations compared to in situ temperatures when incubation waters were collected (compare Figure S9 with Figure 2).

Thus, despite no direct correlation, temperature and light are likely levers on seasonal patterns of Mn oxide concentrations and distributions. Specifically, both mineral and microbial Mn oxidation rates will vary as a function of temperature. S2,53 Many microbes previously associated with Mn oxidation have an optimum temperature range between 20 and 30 °C. Mn oxidation do not grow well outside of their optimum temperature ranges, this could decrease the rate of microbial Mn oxidation. This may explain the lower Mn oxide concentrations observed in November. It is well-known that the activity, composition, and abundance of microbes changes seasonally as a function of temperature.

Variation in light quality and intensity between July and November also likely contributed to these temporal Mn oxide variations. Solar irradiance values decrease by about 60% between September and December at a latitude of 40°N, set which would impact both photochemical and photobiological (e.g., photosynthesis) rates and extents. These seasonally varying light influences are difficult to disentangle from the corresponding temperature changes, which would also influence the activity and composition of microbial communities over this same timeframe.

Manganese Oxide Formation and Reduction Processes. The observed Mn oxide profiles within Siders Pond point to a combination of biotic and abiotic processes, and incubation experiments using waters collected in September were used to characterize these processes in more detail (Figure 5). Only small changes were observed in Mn oxide concentrations in both light and dark filtered water incubations in September, with about 1  $\mu$ M or less changes in Mn oxide

concentrations in light and dark filtered water incubations compared with >3  $\mu$ M changes in Mn oxide concentrations in killed incubations. This finding indicates that aqueous processes only play a minor role in Mn cycling in Siders Pond. More likely, particle-associated processes, potentially encompassing both microbial oxidation and mineral surface catalysis, underpin Mn oxide formation. This finding would be in-line with previous research results.  $^{57}$ 

Within killed water incubations, loss of more than 3  $\mu$ M Mn oxides occurred in the presence of sunlight while net Mn oxide formation of greater than 3  $\mu$ M occurred in the dark (Figure 5). Net formation of Mn oxides in the dark in the absence of microbial activity points to abiotic light-independent, likely mineral-mediated, Mn oxide formation. Net reduction of Mn oxides within the light killed water incubations indicates that photoreduction is also a predominant process controlling Mn oxide levels within the sunlit waters of Siders Pond (Figure 5). This is consistent with accumulation of dissolved Mn in euphotic zones of other water bodies.  $^{34,35}$ 

Unfiltered water incubations were compared to killed water incubations to characterize microbial and mineral-mediated contributions to Mn oxidation. Manganese oxides accumulated to a greater extent within dark unfiltered water incubations than in the light (Figure 5). Yet, enough oxidation occurred within light unfiltered water incubations to offset Mn oxide depletion by photoreduction, unlike in killed water incubations. These observations highlight the importance of biological activity in counterbalancing photoreduction in Siders Pond. Oxidation occurred in both dark and light unfiltered water incubations. This indicates the presence of light-independent microbial Mn oxidation and possibly some Mn oxidation associated with phototrophic activity, which is explored further in the following section.

Comparison of Mn Oxidation in Surface and Chemocline Incubations. To further understand processes within the dynamic surface waters, incubation experiments in September included both surface and chemocline waters (Figure 5). Chemocline water incubations were exposed to surface oxygen levels to assess the processes that would occur at the interface of the chemocline and mixed layer and when chemocline waters are entrained within the mixed layer. While these absolute rates cannot be used to extrapolate rates of Mn oxide formation within the chemocline within Siders Pond directly, they provide insight into the redox reactivity of the different water parcels.

The rate and extent of Mn oxide formation in chemocline waters was about an order of magnitude faster than in the surface waters (note the y-axis difference in Figure 5A) in both light and dark unfiltered water incubations and in dark killed incubations. The in situ concentration of Mn oxides within these chemocline waters was less than half those in the surface waters (Figure 2), and dissolved Mn concentrations were higher than Mn oxide concentrations within the chemocline on the date of water collection (Figure 3). This may be reflective of a substantial community of Mn-oxidizing bacteria at the interface between the chemocline and the epilimnion. It is currently unclear why there was also substantial oxidation of Mn oxides in dark killed incubations despite relatively low initial Mn oxides concentrations. This may be due to the presence of other minerals in the pond that can catalyze the oxidation of Mn. For instance, Mn oxidation by iron oxides and albite has been shown previously.<sup>58</sup> Alternatively, the low

concentrations of Mn oxides present may have been sufficient to catalyze Mn oxidation.

Differences in Mn(II) concentrations between the chemocline and surface waters are not sufficient to explain the almost one order-of-magnitude faster Mn oxidation rates observed in chemocline incubations compared to surface water incubations. In Siders Pond in September, surface concentrations of dissolved Mn were low, but concentrations reached about 10  $\mu$ M within the chemocline. However, because 25  $\mu$ M MnCl<sub>2</sub> was added to all incubation experiments, the initial concentrations of dissolved Mn in chemocline incubations were less than twice those in surface water incubations, meaning dissolved Mn concentrations alone likely did not account for the faster rate of Mn oxidation observed in chemocline incubations. Additional experiments are needed to identify differences between the chemical and biological processes within the surface and chemocline waters.

Furthermore, and as with the surface water incubations, microbial oxidation occurred in addition to mineral-mediated Mn oxidation (compare light killed versus unfiltered chemocline incubations, Figure 5). Given the dynamic nature of the chemocline depth within the pond (Figure 2), reactants such as dissolved Mn and oxygen likely play an important role in the biological cycling of Mn as mixing of oxygen and light penetration depths vary over time. It is notable that the pH increased to 8.99 in unfiltered light chemocline water incubations, while all other incubation experiments stayed at or near pH 8. This high pH is likely associated with phototrophic activity, as photosynthesis would lead to increased pH values<sup>59</sup> like those observed in August and in light incubation experiments throughout the season. However, it is unclear if this biologically mediated Mn oxidation in chemocline waters was due to direct enzymatic or metabolic reactions by microbes, or if the increased favorability of Mn oxidation by O<sub>2</sub> at this higher pH resulting from phototrophic activity also played a role. Notably, this drastic pH change was not observed in unfiltered surface water incubations, which had a final pH of 8.33, yet there was still a small amount of net Mn oxidation, thereby indicating that the pH change alone was not responsible for counteracting photoreduction in unfiltered water incubations.

Factors Influencing Particulate Manganese Mineralogy. In addition to being a predominant factor in Mn oxide formation rates, light also influenced the structure of Mn oxides formed. This was studied using Mn K-edge XAS on unfiltered September incubations, as LBB cannot differentiate between Mn(III) and Mn(IV) oxides. Manganese mineralogy differed as a function of light exposure within unfiltered surface and chemocline incubations after 19 days of incubation. In both surface and chemocline waters, the average oxidation state (AOS) was lower in light incubations than in dark incubations (Figure 6, Table S4). This also led to the presence of up to 50% more reduced Mn oxides phases, such as feitknechtite and triclinic birnessite, in the light chemocline incubations. In contrast, dark chemocline incubations consisted of mostly ( $\sim$ 75%)  $\delta$ -MnO<sub>2</sub> (Figure 6 and Table S4). In combination, these results indicate that the presence of light led not just to dissolved Mn(II) formation, but also production of more-reduced Mn oxide minerals. Birnessite can be reductively transformed into more reduced minerals, like feitknechtite, by aqueous Mn(II);60,61,60,61 thus Mn(II) production as a result of photoreduction likely influenced the resulting Mn mineralogy.

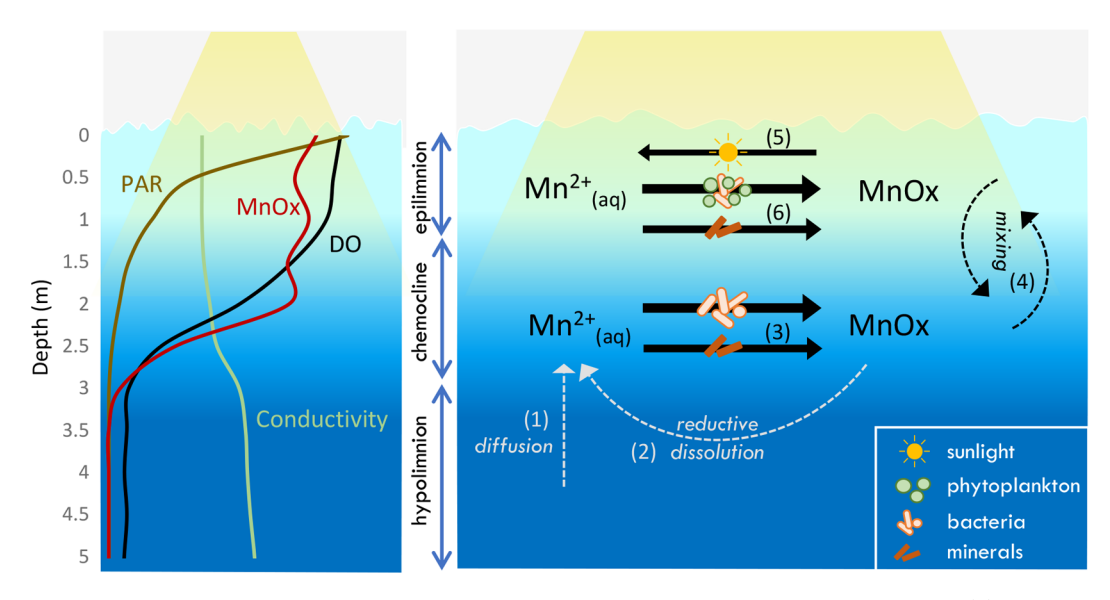


Figure 8. Conceptual figure of the processes underlying Mn cycling in Siders Pond. The numbered processes are: (1) dissolved Mn from deep waters diffuses into the chemocline, (2) reductive dissolution of Mn oxides occurs within the chemocline, (3) microbial and mineral-mediated Mn oxidation occurs at the chemocline-epilimnion interface, (4) mixing of the surface layer keeps Mn oxides evenly distributed throughout the epilimnion, (5) Mn oxides undergo photoreduction at and near the pond surface, and (6) photoreduced Mn is concurrently reoxidized to Mn oxides by microbes and minerals, leading to net Mn oxide accumulation at times. The combined rates of processes (3) and (6) must be greater than the rate of process (5) for Mn oxides to accumulate at the surface.

As in the incubations, particulate Mn in Siders Pond was mainly present as Mn oxides composed predominantly of Mn(IV) (55–79%) with some Mn(III) (12–26%) (Figure 3). EXAFS analysis indicated the presence of birnessite-like phases, including a mineral structurally similar to  $\delta$ -MnO<sub>2</sub>, triclinic birnessite, and asbolane (or another metal-substituted birnessite similar to  $\delta$ -MnO<sub>2</sub>). The AOS varied from roughly 3.15 to 3.75. Excluding Mn(II) to remove particulate manganese that was not associated with Mn oxide minerals yielded more consistent values (between 3.75 and 3.90), with little variation in AOS by depth or date (Figure 3, Table S2). This indicates that changes in AOS were largely driven not by changes in Mn oxide mineralogy, but by differences in the relative Mn(II) content of the particulate Mn, which may be (ad)sorbed to minerals or found on/within microbes. While future explorations could target this more thoroughly, it appears unlikely that Mn(II) is present in Siders Pond as Mn carbonates. The XANES spectrum for our sample from September 17th at a depth of 2.5 m, which was determined to be exclusively Mn(II) using LCF, does not match closely with the XANES spectra of rhodochrosite observed previously. The XANES spectrum of this sample (Figure S11) is missing the feature found at ~6560 eV in the rhodochrosite spectrum as measured by Boulard et al.<sup>62</sup>

Manganese oxides found in aquatic systems are typically characterized as poorly crystalline birnessite phases. 63,64 Birnessite phases of varying symmetry and structure have also been directly associated with Mn oxide production by bacteria and fungi. 49,57 Thus, the Mn(IV) phases in Siders Pond and found in our dark unfiltered incubation experiment are consistent with those within other natural systems and produced biologically. 49,65 Additionally, the occurrence of more reduced Mn oxides like feitknechtite and triclinic birnessite within XAS samples from the pond, which were present in substantial fractions in light unfiltered incubations but not dark unfiltered incubations, indicates that photo-

reduction likely also plays a role in Mn mineralogy in Siders Pond.

**Conceptual Framework.** Siders Pond has a dynamic Mn cycle, evidenced by the observed changes in Mn profiles and water incubations over the course of a summer to fall transition. A conceptual framework for this dynamic Mn cycle is presented in Figure 8. Dissolved Mn concentrations were generally highest within the hypolimnion and, through upward diffusion, are likely the primary contributor of dissolved manganese into the chemocline (Figure 2). Based on chemocline incubations (Figure 5), and the presence of Mn oxides slightly below the boundary between the epilimnion and the chemocline, it appears that both microbial and mineralmediated oxidation of Mn(II) occur within the chemocline near the chemocline-epilimnion interface. Relatively constant Mn oxide concentrations extending from the surface of the pond to the top of the chemocline indicates that the epilimnion is well-mixed on relatively short time scales.

While net accumulation of Mn oxides is evident throughout the epilimnion between the late summer and early fall, several processes seem to simultaneously promote both Mn oxidation and reduction. Based on incubation experiments of surface waters (see Figure 5 and 7), both mineral-mediated and microbially mediated Mn oxidation occur. However, photoreduction outpaces mineral-mediated oxidation alone (compare killed light and dark rates in Figure 7), and additional contributions from microbially mediated oxidation leads to Mn oxide formation (compare unfiltered light and killed light oxidation rates in Figure 7). We propose that the relative contributions of these processes vary throughout the season, due to changes in light and temperature, and cause variations in Mn oxide concentrations within Siders Pond.

Broader Context and Future Research Directions. While this research provides additional evidence for the presence of substantial concentrations of Mn oxides in nonmarine surface waters, more work is needed to understand why surface water Mn oxides are more commonly found in

fresh and brackish than marine waters. This may be due to differences in microbial Mn oxidation and/or Mn photoreduction rates between marine and inland waters. Differences in particle sinking may also play a role because Mn oxides flocculate at higher salinity. Furthermore, light attenuation depths are much deeper in the open ocean than inland water bodies. The euphotic zone in the ocean can be between 30–100 m deep, while in Siders Pond, the euphotic zone was less than 5 m deep (Figure 2F). This could explain the greater relative importance of photoreduction in marine systems, as light is attenuated more gradually, allowing for photoreduction deeper in the water column despite similar solar irradiances.

Differences in microbial communities between water bodies may also contribute to differences in net oxidation rates. Yet, the lack of specific organisms and/or conserved genes broadly involved in Mn oxidation makes it difficult to determine how differences in microbial community composition may lead to differences in Mn oxidation rates in the environment. Notably, microbial abundances are generally much lower in the ocean than in inland water bodies, with 103 to 106 cells/mL in seawater<sup>68</sup> compared to  $\sim 2-5 \times 10^6$  cells/mL in the surface waters of lakes.<sup>69</sup> This may lead to lower microbial oxidation rates in seawater even if cell-specific Mn oxidation rates are similar. Additionally, higher organic matter concentrations may influence microbial growth or lead to more direct interactions with Mn; marine DOC concentrations in one study were found to range between 40 and 115  $\mu$ M<sup>70</sup> while the surface water DOC concentrations in Siders Pond over the course of this work were between 165 and 270  $\mu$ M (Figure S6). Moving forward, systematic targeted incubations will help identify the factors controlling microbes involved in Mn oxide formation and cycling in Siders Pond. More research is needed to understand how the processes governing Mn cycling in Siders Pond change over longer time scales and how the relative importance of the processes considered in this work affect other brackish and freshwater bodies.

Our data helped identify a suite of light-dependent and -independent reactions that influence Mn oxide concentrations within a coastal meromictic pond. Particle-mediated processes are likely the largest contributors to Mn oxidation in Siders Pond. Based on incubation experiments, particle-mediated processes include abiotic (likely mineral-mediated) and biologically associated oxidation. Mn oxide reduction is driven predominantly by photoreduction. Changes in observed Mn oxide concentrations in Siders Pond between July and November are likely driven by changes in these competing particle-mediated oxidation and photoreduction processes. Our results provide new insights into the processes that promote Mn oxide accumulation in aquatic settings.

# ASSOCIATED CONTENT

#### Supporting Information

The Supporting Information is available free of charge at https://pubs.acs.org/doi/10.1021/acsearthspace-chem.2c00368.

Additional characterization, statistical analyses, measurements, and data (PDF)

# AUTHOR INFORMATION

#### **Corresponding Author**

Colleen M. Hansel – Department of Marine Chemistry and Geochemistry, Woods Hole Oceanographic Institution, Woods Hole, Massachusetts 02543, United States; oorcid.org/0000-0002-3506-7710; Email: chansel@whoi.edu

#### Authors

Hayley J. Gadol — Department of Civil and Environmental Engineering, Massachusetts Institute of Technology, Cambridge, Massachusetts 02139, United States; Present Address: H. J. G, Gradient Corp., One Beacon St, Boston, MA, 02108; orcid.org/0000-0002-9019-6275

Chadlin M. Ostrander – Department of Marine Chemistry and Geochemistry, Woods Hole Oceanographic Institution, Woods Hole, Massachusetts 02543, United States

Luciana Villarroel — Department of Marine Chemistry and Geochemistry, Woods Hole Oceanographic Institution, Woods Hole, Massachusetts 02543, United States; Department of Earth, Atmospheric, and Planetary Sciences, Massachusetts Institute of Technology, Cambridge, Massachusetts 02139, United States

Lina Taenzer – Department of Marine Chemistry and Geochemistry, Woods Hole Oceanographic Institution, Woods Hole, Massachusetts 02543, United States; Department of Earth, Atmospheric, and Planetary Sciences, Massachusetts Institute of Technology, Cambridge, Massachusetts 02139, United States

Scott D. Wankel – Department of Marine Chemistry and Geochemistry, Woods Hole Oceanographic Institution, Woods Hole, Massachusetts 02543, United States

**Véronique E. Carignan** – Sea Education Association, Falmouth, Massachusetts 02540, United States

Complete contact information is available at: https://pubs.acs.org/10.1021/acsearthspacechem.2c00368

# **Author Contributions**

H.J.G. and C.M.H. conceptualized the research. H.J.G., C.M.H., C.M.O., L.V., L.T., S.D.W., and V.E.O. performed the fieldwork. H.J.G., C.M.O., and L.V. carried out sample analyses. H.J.G. analyzed the data set. H.J.G. and C.M.H. wrote the paper with contributions from C.M.O., L.V., L.T., S.D.W., and V.E.O.

#### **Funding**

This project was supported by NSF-OCE 1924236 (to C.M.H., V.E.O., S.D.W.), NSF-EAR 2025853 (to C.M.H.), and NSF-EAR 2129034 (to C.M.O., C.M.H.). The MIT Department of Civil and Environmental Engineering provided funding for H.J.G.

#### Notes

The authors declare no competing financial interest.

# ACKNOWLEDGMENTS

The authors are grateful to Tristan Horner for contributions and insight during previous field seasons that were not included in this work. We are also grateful to Joe Vallino for helping initially coordinate boat access to Siders Pond. We are thankful to Kalina Grabb and Sam Bowman for additional help with field sampling. We would like to thank the local Siders Pond community for insightful conversations about and access to the pond. The authors are also grateful to Ryan Davis for helping us with running XAS samples remotely at SSRL, and to Gretchen Swarr for assistance in generating data on the ICPMS. We would also like to thank the three anonymous reviewers and the editor for providing comments that improved the quality of this manuscript. The contents of this

manuscript were also incorporated in a PhD dissertation accepted by Massachusetts Institute of Technology.<sup>71</sup>

# ABBREVIATIONS

Mn, manganese; ROS, reactive oxygen species; AOS, average oxidation state; Fe, Iron; NO, Nitric oxide; ICPMS, Inductively Coupled Plasma Mass Spectrometer; PAR, photosynthetically active radiation; XANES, X-ray absorption near edge structure; EXAFS, extended X-ray absorption fine structure

# REFERENCES

- (1) McKeown, D. A.; Post, J. E. Characterization of Manganese Oxide Mineralogy in Rock Varnish and Dendrites Using X-Ray Absorption Spectroscopy. *Am. Mineral.* **2001**, 86 (5–6), 701–713.
- (2) Post, J. E. Manganese Oxide Minerals: Crystal Structures and Economic and Environmental Significance. *Proc. Natl. Acad. Sci. U. S. A.* 1999, 96 (7), 3447–3454.
- (3) Hein, J. R.; Koschinsky, A. Deep-Ocean Ferromanganese Crusts and Nodules. *Treatise on Geochemistry: Second Edition* **2014**, *13*, 273–291.
- (4) Sutherland, K. M.; Wankel, S. D.; Hein, J. R.; Hansel, C. M. Spectroscopic Insights Into Ferromanganese Crust Formation and Diagenesis. *Geochemistry, Geophysics, Geosystems* **2020**, 21 (11), No. e2020GC009074.
- (5) Tani, Y.; Ohashi, M.; Miyata, N.; Seyama, H.; Iwahori, K.; Soma, M. Sorption of Co(II), Ni(II), and Zn(II) on Biogenic Manganese Oxides Produced by a Mn-Oxidizing Fungus, Strain KR21–2. *J. Environ. Sci. Health A Tox Hazard Subst Environ. Eng.* **2004**, 39 (10), 2641–2660.
- (6) Loganathan, P.; Burau, R. G. Sorption of Heavy Metal Ions by a Hydrous Manganese Oxide. *Geochim. Cosmochim. Acta* **1973**, *37* (5), 1277–1293.
- (7) Wick, S.; Peña, J.; Voegelin, A. Thallium Sorption onto Manganese Oxides. *Environ. Sci. Technol.* **2019**, *53*, 13168.
- (8) Wang, Y.; Feng, X.; Villalobos, M.; Tan, W.; Liu, F. Sorption Behavior of Heavy Metals on Birnessite: Relationship with Its Mn Average Oxidation State and Implications for Types of Sorption Sites. *Chem. Geol.* **2012**, 292–293, 25–34.
- (9) Browning, T. J.; Achterberg, E. P.; Engel, A.; Mawji, E. Manganese Co-Limitation of Phytoplankton Growth and Major Nutrient Drawdown in the Southern Ocean. *Nature Communications* **2021**, *12* (1), 1–9.
- (10) Sunda, W. G.; Kieber, D. J. Oxidation of Humic Substances by Manganese Oxides Yields Low-Molecular-Weight Organic Substrates. *Nature* **1994**, *367* (6458), 62–64.
- (11) Lovley, D. R.; Phillips, E. J. Novel Mode of Microbial Energy Metabolism: Organic Carbon Oxidation Coupled to Dissimilatory Reduction of Iron or Manganese. *Appl. Environ. Microbiol.* **1988**, *54* (6), 1472–1480.
- (12) Byrne, R. H. Inorganic Speciation of Dissolved Elements in Seawater: The Influence of PH on Concentration Ratios. *Geochem Trans* **2002**, 3 (1), 11.
- (13) Oldham, V. E.; Owings, S. M.; Jones, M. R.; Tebo, B. M.; Luther, G. W. Evidence for the Presence of Strong Mn(III)-Binding Ligands in the Water Column of the Chesapeake Bay. *Mar Chem.* **2015**, *171*, 58–66.
- (14) Madison, A. S.; Tebo, B. M.; Mucci, A.; Sundby, B.; Luther, G. W. Abundant Porewater Mn(III) Is a Major Component of the Sedimentary Redox System. *Science* (1979) **2013**, 341 (6148), 875–878.
- (15) Luther, G. W. The Role of One- and Two-Electron Transfer Reactions in Forming Thermodynamically Unstable Intermediates as Barriers in Multi-Electron Redox Reactions. *Aquat Geochem* **2010**, *16* (3), 395–420.
- (16) Duckworth, O. W.; Sposito, G. Siderophore-Manganese (III) Interactions. I. Air-Oxidation of Manganese (II) Promoted by Desferrioxamine B. *Environ. Sci. Technol.* **2005**, 39 (16), 6037–6044.

- (17) Shoiful, A.; Ohta, T.; Kambara, H.; Matsushita, S.; Kindaichi, T.; Ozaki, N.; Aoi, Y.; Imachi, H.; Ohashi, A. Multiple Organic Substrates Support Mn(II) Removal with Enrichment of Mn(II)-Oxidizing Bacteria. *J. Environ. Manage* **2020**, 259, No. 109771.
- (18) Sunda, W. G.; Huntsman, S. A. Photoreduction of Manganese Oxides in Seawater. *Mar Chem.* **1994**, *46* (1–2), 133–152.
- (19) Hansel, C. M.; Zeiner, C. A.; Santelli, C. M.; Webb, S. M. Mn(II) Oxidation by an Ascomycete Fungus Is Linked to Superoxide Production during Asexual Reproduction. *Proc. Natl. Acad. Sci. U. S. A.* **2012**, *109* (31), 12621–12625.
- (20) Nico, P. S.; Anastasio, C.; Zasoski, R. J. Rapid Photo-Oxidation of Mn(II) Mediated by Humic Substances. *Geochim. Cosmochim. Acta* **2002**, *66* (23), 4047–4056.
- (21) Garg, S.; Rose, A. L.; Waite, T. D. Photochemical Production of Superoxide and Hydrogen Peroxide from Natural Organic Matter. *Geochim. Cosmochim. Acta* **2011**, 75 (15), 4310–4320.
- (22) Zhang, D.; Yan, S.; Song, W. Photochemically Induced Formation of Reactive Oxygen Species (ROS) from Effluent Organic Matter. *Environ. Sci. Technol.* **2014**, *48* (21), 12645–12653.
- (23) Marshall, J. A.; Ross, T.; Pyecroft, S.; Hallegraeff, G. Superoxide Production by Marine Microalgae: II. Towards Understanding Ecological Consequences and Possible Functions. *Mar Biol.* **2005**, 147 (2), 541–549.
- (24) Diaz, J. M.; Hansel, C. M.; Voelker, B. M.; Mendes, C. M.; Andeer, P. F.; Zhang, T. Widespread Production of Extracellular Superoxide by Heterotrophic Bacteria. *Science* (1979) **2013**, 340 (6137), 1223–1226.
- (25) Johnson, J. E.; Savalia, P.; Davis, R.; Kocar, B. D.; Webb, S. M.; Nealson, K. H.; Fischer, W. W. Real-Time Manganese Phase Dynamics during Biological and Abiotic Manganese Oxide Reduction. *Environ. Sci. Technol.* **2016**, *50* (8), 4248–4258.
- (26) Ma, D.; Wu, J.; Yang, P.; Zhu, M. Coupled Manganese Redox Cycling and Organic Carbon Degradation on Mineral Surfaces. *Environ. Sci. Technol.* **2020**, *54* (14), 8801–8810.
- (27) Flynn, E. D.; Catalano, J. G. Reductive Transformations of Layered Manganese Oxides by Small Organic Acids and the Fate of Trace Metals. *Geochim. Cosmochim. Acta* **2019**, 250, 149–172.
- (28) Schaefer, M. v.; Handler, R. M.; Scherer, M. M. Fe(II) Reduction of Pyrolusite ( $\beta$ -MnO2) and Secondary Mineral Evolution. *Geochem Trans* **2017**, *18* (1), 1–11.
- (29) Burdige, D. J.; Nealson, K. H. Chemical and Microbiological Studies of Sulfide-mediated Manganese Reduction. *Geomicrobiol J.* **1986**, *4* (4), 361–387.
- (30) Godwin, C. M.; Zehnpfennig, J. R.; Learman, D. R. Biotic and Abiotic Mechanisms of Manganese (II) Oxidation in Lake Erie. *Front Environ. Sci.* **2020**, *8*, 57.
- (31) Zhang, Y.; del Vecchio, R.; Blough, N. v. Investigating the Mechanism of Hydrogen Peroxide Photoproduction by Humic Substances. *Environ. Sci. Technol.* **2012**, *46* (21), 11836–11843.
- (32) Marafatto, F. F.; Strader, M. L.; Gonzalez-Holguera, J.; Schwartzberg, A.; Gilbert, B.; Peña, J. Rate and Mechanism of the Photoreduction of Birnessite (MnO2) Nanosheets. *Proc. Natl. Acad. Sci. U. S. A.* **2015**, *112* (15), 4600–4605.
- (33) Oldham, V. E.; Lamborg, C. H.; Hansel, C. M. The Spatial and Temporal Variability of Mn Speciation in the Coastal Northwest Atlantic Ocean. *J. Geophys Res. Oceans* **2020**, *125* (1), No. e2019JC015167, DOI: 10.1029/2019JC015167.
- (34) Beck, M.; Dellwig, O.; Schnetger, B.; Riedel, T.; Brumsack, H. J. Manganese Dynamics in Tidal Basins of the Wadden Sea: Spatial/Seasonal Patterns and Budget Estimates. *Mar Chem.* **2020**, 225, 103847.
- (35) Sunda, W. G.; Huntsman, S. A. Effect of Sunlight on Redox Cycles of Manganese in the Southwestern Sargasso Sea. *Deep Sea Research Part A, Oceanographic Research Papers* 1988, 35 (8), 1297–1317.
- (36) Sunda, W. G.; Huntsman, S. A.; Harvey, G. R. Photoreduction of Manganese Oxides in Seawater and Its Geochemical and Biological Implications. *Nature* **1983**, *301* (5897), 234–236.

- (37) Sunda, W. G.; Huntsman, S. A. Diel Cycles in Microbial Manganese Oxidation and Manganese Redox Speciation in Coastal Waters of the Bahama Islands. *Limnol Oceanogr* **1990**, 35 (2), 325–338.
- (38) Xiang, Y.; Lam, P. J.; Lee, J. M. Diel Redox Cycle of Manganese in the Surface Arctic Ocean. *Geophys. Res. Lett.* **2021**, 48 (23), No. e2021GL094805.
- (39) Oldham, V. E.; Jones, M. R.; Tebo, B. M.; Luther, G. W. Oxidative and Reductive Processes Contributing to Manganese Cycling at Oxic-Anoxic Interfaces. *Mar Chem.* **2017**, *195*, 122–128.
- (40) Altmann, H. J. Bestimmung von in Wasser Gelöstem Sauerstoff Mit Leukoberbelinblau I Eine Schnelle Winkler-Methode. Zeitschrift für Analytische Chemie 1972, 262 (2), 97–99.
- (41) Jones, M. R.; Luther, G. W.; Mucci, A.; Tebo, B. M. Concentrations of Reactive Mn(III)-L and MnO2 in Estuarine and Marine Waters Determined Using Spectrophotometry and the Leuco Base, Leucoberbelin Blue. *Talanta* **2019**, 200, 91–99.
- (42) Stookey, L. L. Ferrozine—a New Spectrophotometric Reagent for Iron. *Anal. Chem.* **1970**, *42* (7), 779–781.
- (43) Cline, J. D. Spectrophotometric Determination of Hydrogen Sulfide in Natural Waters. *Limnol Oceanogr* **1969**, *14* (3), 454–458.
- (44) Garside, C. A Chemiluminescent Technique for the Determination of Nanomolar Concentrations of Nitrate and Nitrite in Seawater. *Mar Chem.* 1982, 11 (2), 159–167.
- (45) Pai, S.-C.; Yang, C.-C.; P. Riley, J. Formation Kinetics of the Pink Azo Dye in the Determination of Nitrite in Natural Waters. *Anal. Chim. Acta* **1990**, 232 (C), 345–349.
- (46) Learman, D. R.; Wankel, S. D.; Webb, S. M.; Martinez, N.; Madden, A. S.; Hansel, C. M. Coupled Biotic—Abiotic Mn(II) Oxidation Pathway Mediates the Formation and Structural Evolution of Biogenic Mn Oxides. *Geochim. Cosmochim. Acta* **2011**, 75 (20), 6048–6063.
- (47) Webb, S. M. SIXpack: A Graphical User Interface for XAS Analysis Using IFEFFIT. *Physica Scripta T* **2005**, *T115* (T115), 1011–1014.
- (48) Caraco, N. Phosphorus, Iron, and Carbon Cycling in a Salt Stratified Coastal Pond. PhD Thesis, Boston University, 1986. h t t p s://www.proquest.com/openview/0d094956f4e4fd3d96904fb14e3ddd42/1?pq-origsite=gscholar&cbl=18750&diss=y (accessed 2022-09-29).
- (49) Webb, S. M.; Tebo, B. M.; Bargar, J. R. Structural Characterization of Biogenic Mn Oxides Produced in Seawater by the Marine Bacillus Sp. Strain SG-1. *Am. Mineral.* **2005**, *90* (8–9), 1342–1357.
- (50) Santelli, C. M.; Webb, S. M.; Dohnalkova, A. C.; Hansel, C. M. Diversity of Mn Oxides Produced by Mn(II)-Oxidizing Fungi. *Geochim. Cosmochim. Acta* **2011**, *75* (10), 2762–2776.
- (51) Vallino, J. J.; Huber, J. A. Using Maximum Entropy Production to Describe Microbial Biogeochemistry over Time and Space in a Meromictic Pond. *Front. Environ. Sci.* **2018**, *6* (OCT), 100.
- (52) Hem, J. D.; Lind, C. J. Nonequilibrium Models for Predicting Forms of Precipitated Manganese Oxides. *Geochim. Cosmochim. Acta* **1983**, *47* (11), 2037–2046.
- (53) Tebo, B. M.; Emerson, S. Effect of Oxygen Tension, Mn(II) Concentration, and Temperature on the Microbially Catalyzed Mn(II) Oxidation Rate in a Marine Fjord. *Appl. Environ. Microbiol.* **1985**, 50 (5), 1268–1273.
- (54) Kent, A. G.; Garcia, C. A.; Martiny, A. C. Increased Biofilm Formation Due to High Temperature Adaptation in Marine Roseobacter. *Nat. Microbiol* **2018**, 3 (9), 989.
- (55) Wilhelm, S. W.; Lecleir, G. R.; Bullerjahn, G. S.; Mckay, R. M.; Saxton, M. A.; Twiss, M. R.; Bourbonniere, R. A. Seasonal Changes in Microbial Community Structure and Activity Imply Winter Production Is Linked to Summer Hypoxia in a Large Lake. *FEMS Microbiol Ecol* **2014**, *87* (2), 475–485.
- (56) Apell, J. N.; McNeill, K. Updated and Validated Solar Irradiance Reference Spectra for Estimating Environmental Photodegradation Rates. *Environ. Sci. Process Impacts* **2019**, 21 (3), 427–437.

- (57) Tebo, B. M.; Bargar, J. R.; Clement, B. G.; Dick, G. J.; Murray, K. J.; Parker, D.; Verity, R.; Webb, S. M. Biogenic Manganese Oxides: Properties and Mechanisms of Formation. *Annu. Rev. Earth Planet Sci.* **2004**, *32*, 287–328.
- (58) Junta, J. L.; Hochella, M. F. Manganese (II) Oxidation at Mineral Surfaces: A Microscopic and Spectroscopic Study. *Geochim. Cosmochim. Acta* 1994, 58 (22), 4985.
- (59) Axelsson, L. Changes in PH as a Measure of Photosynthesis by Marine Macroalgae. *Marine Biology* 1988 97:2 1988, 97 (2), 287–294.
- (60) Hinkle, M. A. G.; Flynn, E. D.; Catalano, J. G. Structural Response of Phyllomanganates to Wet Aging and Aqueous Mn(II). *Geochim. Cosmochim. Acta* **2016**, 192, 220–234.
- (61) Elzinga, E. J. Reductive Transformation of Birnessite by Aqueous Mn(II). *Environ. Sci. Technol.* **2011**, 45 (15), 6366–6372.
- (62) Boulard, E.; Liu, Y.; Koh, A. L.; Reagan, M. M.; Stodolna, J.; Morard, G.; Mezouar, M.; Mao, W. L. Transformations and Decomposition of MnCO3 at Earth's Lower Mantle Conditions. *Front Earth Sci. (Lausanne)* **2016**, *4*, 1–9.
- (63) Jones, C.; Crowe, S. A.; Sturm, A.; Leslie, K. L.; MacLean, L. C. W.; Katsev, S.; Henny, C.; Fowle, D. A.; Canfield, D. E. Biogeochemistry of Manganese in Ferruginous Lake Matano. *Indonesia. Biogeosciences* **2011**, *8* (10), 2977–2991.
- (64) Hermans, M.; Astudillo Pascual, M.; Behrends, T.; Lenstra, W. K.; Conley, D. J.; Slomp, C. P. Coupled Dynamics of Iron, Manganese, and Phosphorus in Brackish Coastal Sediments Populated by Cable Bacteria. *Limnol Oceanogr* **2021**, *66*, 2611.
- (65) Villalobos, M.; Toner, B.; Bargar, J.; Sposito, G. Characterization of the Manganese Oxide Produced by Pseudomonas Putida Strain MnB1. *Geochim. Cosmochim. Acta* **2003**, *67* (14), 2649–2662.
- (66) Toyoda, K.; Tebo, B. M. The Effect of Ca2+ Ions and Ionic Strength on Mn(II) Oxidation by Spores of the Marine Bacillus Sp. SG-1. *Geochim. Cosmochim. Acta* **2013**, *101*, 1–11.
- (67) Lorenzen, C. J. Extinction of Light in the Ocean by Phytoplankton. ICES Journal of Marine Science 1972, 34 (2), 262-
- (68) Tabor, P. S.; Ohwada, K.; Colwell, R. R. Filterable Marine Bacteria Found in the Deep Sea: Distribution, Taxonomy, and Response To. *Ecology* **1981**, *7* (1), 67–83.
- (69) Garcia-Chaves, M. C; Cottrell, M. T; Kirchman, D. L; Ruiz-Gonzalez, C.; del Giorgio, P. A Single-Cell Activity of Freshwater Aerobic Anoxygenic Phototrophic Bacteria and Their Contribution to Biomass Production. *ISME J.* **2016**, *10* (7), 1579.
- (70) Fry, B.; Peltzer, E. T.; Hopkinson, C. S.; Nolin, A.; Redmond, L. Analysis of Marine DOC Using a Dry Combustion Method. *Mar Chem.* **1996**, 54 (3–4), 191–201.
- (71) Gadol, H. J. Cycling of Iron and Manganese (Oxyhydr)Oxides in the Presence of Organic Matter. PhD Thesis, Massachusetts Institute of Technology, 2021.